# Pre-Yielding and Necking Process of Double Network Hydrogels Revealed by Sample Geometry Effects

Masahiro Yoshida[a], Ryuji Kiyama[b,c*], Ye Zhang[a], Daniel R. King[b], Takayuki Kurokawa[b], Jian Ping Gong[b,d*]

[a]Graduate School of Life Science, Hokkaido University, N21W11, Kita-ku, Sapporo 001-0021, Japan;

[b]Faculty of Advanced Life Science, Hokkaido University, N21W11, Kita-ku, Sapporo 001-0021, Japan;

[c]Creative Research Institution (CRIS), Hokkaido University, N21W11, Kita-ku, Sapporo 001-0021, Japan;

[d]Institute for Chemical Reaction Design and Discovery (WPI-ICReDD), Hokkaido University, N21W10, Kita-ku, Sapporo 001-0021, Japan

Corresponding authors: r.kiyama@sci.hokudai.ac.jp; gong@sci.hokudai.ac.jp

## Abstract

Understanding the yielding and necking mechanisms of double network (DN) materials is crucial for establishing structure-property correlations. While previous studies have primarily

focused on how macro-yielding behavior changes with network structure and swelling, in this work, we study the local internal damage in the pre-yielding process to unveil the yielding and necking mechanisms for typical DN gels. Through birefringence retardation imaging during tensile deformation on DN gels of various sample geometries, our findings reveal the following key points: 1) Initiation and Growth of Damage Zones: Prior to macroscopic yielding, damage zones initiate from the sample edges and gradually grow towards the sample center with elongation. 2) Rapid Propagation and Yielding: Beyond a certain stress threshold, damage zones rapidly propagate under constant loading. Two damage zones eventually merge at the sample center, resulting in yielding. 3) Intrinsic Stress Determination: The stress at this point is intrinsic and determined by the structure of the two networks. 4) Pseudo Size-Dependency: Samples with insufficient width exhibit a pseudo size-dependency of yielding stress, as yielding occurs before reaching the critical stress. To explain the origin of intrinsic yielding stress, we introduce an intrinsic effective crack length ($c_I$) as a measure of stress concentration around the internal crack tip of the damaged zone in the first network. Beyond this length, the influence on internal stress concentration around the damage zone is effectively screened by the load-bearing effect of the stretchable second network. The estimated $c_I$, dependent on the microstructure of the two networks, was approximately 10 times the mesh size of the first network for typical DN gels.

**Keywords:**

Double Network Hydrogels, Yielding, Sample Geometry, Stress Concentration, Damage Zone, Birefringence Images

## 1. Introduction

Hydrogels are hydrophilic polymer networks that can significantly swell in water, resulting in an elastic solid with high water content. Because of their similarities to the tissues that make up living organisms, there has been widespread interest in their application as artificial biomaterials; however, their weak mechanical properties limit their potential application range. Fortunately, over the last 20 years, several mechanically strong or tough hydrogels have been developed, including double network (DN) gels [1–3], nanocomposite gels [4–6], tetra-PEG gels [7–9], and slide-ring gels [10–12]. Notably, DN gels exhibit extremely high strength and toughness despite containing up to 90% water by mass. DN gels are composed of two asymmetric networks: the first network, made of short chains, is hard/brittle and ruptures at low strain and (relatively) low stress; and the second network, made of long chains, is

54 soft/stretchable and ruptures at high strain and (relatively) high stress. When force is applied to
55 DN gels, the first network chains preferentially break over wide ranges (damage zones),
56 whereas the second network chains carry the broken first network chains' load, suppressing
57 local stress amplification on the first network and preventing global material fracture [13–16].
58 This internal fracture mechanism leads to the dissipation of a large amount of energy at the
59 crack tip through the formation of a damage zone, which enhances strength and toughness.

60 The DN gel's unique internal fracture mechanism results in a yielding-like phenomenon
61 accompanied by necking during uniaxial stretching [17,18]. The material exhibits
62 inhomogeneous macroscale deformation beyond the yielding stretch by forming a necked zone.
63 The necked zone propagates by stretching the sample with an almost constant applied force
64 until the entire sample is necked. Subsequently, the applied force increases again with further
65 stretching.

66 Because yielding is an important feature of tough DN gels, many researchers have
67 experimentally [18–20] and theoretically [21–24] studied the yielding mechanism. By studying
68 the yielding behaviors of DN gels with varied first network pre-swelling ratios, the yielding
69 point, at which the applied stress reaches the local maximum with the applied stretch, is found
70 to be proportional to the stretch limit of the first network strands, and the yielding stress is
71 proportional to the first network strand areal density [18,20].

In terms of fracture mechanics, the inclusion of the second network in the DN gels significantly reduces the fracture singularity (stress concentration) of the brittle first network. The yielding stress of DN gels typically exceeds the breaking stress of the single first network alone by a factor of 100, highlighting the enhanced robustness of the double network structure, especially in contrast to the heightened flaw sensitivity exhibited by the single first network. The question that emerges is what governs the yielding stress of the DN gels and to what extent the stress concentration around the crack in the first network is dampened by the second network. Our findings reveal that the yielding stress falls within in the range of 5–10% of the ideal fracture stress of the first network, as predicted in cases where the stress concentration effect is absent [18,20]. It is worthy to note that, the relatively low yielding stress cannot be solely attributed to the heterogeneity of the first network, as even DN gels with homogeneous first network exhibited a comparable decrease in yield stress [18]. In light of this observation, we posit two potential explanations for the decrease in yielding stress. The first involves the influence of bulk geometry, specifically macroscopic stress concentration. The damage zone at the crack tip of a notched DN materials can extend to values ranging from 100 to 1000 μm [17,25,26]. The magnitude of internal damage of un-notched DN gels preceding yielding could surpass this size significantly and exceed the sample dimensions employed in prior studies, consequently leading to a yielding stress less than the intrinsic one. Such geometric effects on

yielding have been overlooked in previous studies. The second explanation is the influence of molecular structure, involving the microscopic stress concentration. Even after eliminating the macroscopic effect, stress concentration may still persist around the internal crack tip of the first network, resulting in an intrinsic yielding stress lower than the ideal fracture stress of the first network. The former effect can be investigated by changing the geometry of the DN gels, specifically the sample width, while the latter effect can be observed by varying the composition of the DN gels.

In this study, we investigated the pre-yielding behavior of typical DN gels with varying sample geometries and network compositions through uniaxial tensile tests and real-time birefringence retardation measurements. These experiments enabled us to observe the initiation and growth process of the internal damage zone up to the yielding point, shedding light on the role of the second network in supporting the load and mitigating stress concentration around the damage zone tip. To quantify internal stress concentration, we introduced an intrinsic effective crack length ($c_I$) at the DN gel yielding. Utilizing nonlinear elastic fracture mechanics, we estimated $c_I$ from the intrinsic yielding point determined in samples with sufficient width. The outcomes of this study offer a comprehensive understanding of the yielding process in DN gels, laying the groundwork for the development of more robust and resilient gel materials.

## 2. Materials and Methods

### 2.1. Preparation of DN gels.

DN hydrogels comprising poly(2-Acrylamido-2-methylpropanesulfonic acid) (PAMPS) as the first network and poly(*N*,*N*-Dimethylacrylamide) (PDMAAm) as the second network were synthesized following established procedures [27]. Both networks were chemically crosslinked by *N*, *N*′-Methylenebisacrylamide (MBAA). The first network precursor solution was prepared by dissolving AMPS, MBAA, and 2-oxoglutaric acid (α-keto) in pure water. This solution was poured into a reaction mold consisting of a pair of glass plates separated by a silicone spacer (ranging from 0.3 mm to2.0 mm thick) and then exposed to UV light (peak wavelength of 365 nm) within a sealed argon glovebox for 6 h, resulting in the formation of PAMPS gels. The PAMPS gels were then immersed for 1 d in the second network precursor solution, composed of DMAAm, MBAA, and α-keto in pure water. The PAMPS gel was then sandwiched between two glass plates, and exposed to UV light in a sealed argon glovebox for 8 h to yield sheet-like DN gels. The thickness of the DN gels (*t*) was controlled by the thickness of the silicone spacer used during the synthesis of the PAMPS gels. The compositions used for the synthesis of the DN gels are detailed in **Table 1**. Throughout the study, variations in the crosslinker concentration in the first network and the monomer concentration in the second network were explored. In **Table 1**, the mol% values are relative to the corresponding monomer concentration.

126 The DN gel samples were denoted as DN*X*-*Y* (*X*: MBAA crosslinker concentration in the first
127 network, *Y*: DMAAm monomer concentration in the second network). Mechanical
128 measurements were conducted on the DN gels in their as-prepared state.

129 **Table 2** displays the mechanical and structure parameters of the first network. The Young's
130 modulus ($E_0$) of the as-prepared first network was determined through indentation tests using a
131 rigid sphere indenter [28]. These tests were conducted with a mechanical tester (AGX-V,
132 Shimadzu Co., Japan) at a compression strain rate of $1/600\mathrm{s}^{-1}$. $E_0$ was estimated from the
133 initial slopes of the compressive stress-strain curves. The number of monomer units between
134 two crosslinks ($N$) was estimated using the equation [29],

135 $$E_0 = \frac{3C_0 k_B T}{N}, \qquad (1)$$

136 where $C_0$, $k_B$, and $T$ denote polymer concentration, the Boltzmann constant, and temperature,
137 respectively. In our calculation for $N$, we assumed that all of the AMPS monomers in the
138 precursor solutions were converted into the mechanically effective network, resulting in $C_0 \simeq$
139 1 M ($M = 6.02 \times 10^{26}\ \mathrm{m}^{-3}$). The $N$ thus estimated represents an approximation of upper bound
140 limit, assuming the absence of dangling chains or loops in the polymer network. In reality, for
141 a PAMPS network formed from 1 M monomer and 1 mol% crosslinker, our TEM observations
142 on the network structure revealed that only about 30% of the monomers contribute to

mechanically effective chains [30]. Considering the crosslinker concentration in the current study is 2~4 mol%, higher than 1 mol%, we posit that the percentage of monomers forming mechanically effective networks is likely elevated, ranging from approximately 40 to 60%. When factoring in this adjustment, the mesh size calculated using this method closely aligns with values observed from TEM images [30]. The average mesh size of the as-prepared first network gel ($R_0$) was estimated from the relationship [29],

$$R_0 \simeq b_k\sqrt{N_k} = \sqrt{Nab_k}, \qquad (2)$$

where $N_k$ represents number of Kuhn monomer units between two crosslinks, $a$ and $b_k$ represent the monomer length and Kuhn monomer length, respectively. We adopted the Kuhn monomer length $b_k$ = 0.5 nm and $a$ = 0.25 nm for PAMPS based on the literature [31]. Linear swelling ratio ($\lambda_s$) of the first network within the DN gels was estimated from the thickness ratio of the as-prepared DN gel to that of the as-prepared first network. The first network mesh size ($R$) in the as-prepared DN gels was estimated as follows assuming the affine deformation,

$$R = R_0 \times \lambda_s \qquad (3)$$

**Table 1.** Composition for the synthesis of DN gels coded as DN*X*-*Y*.

| First network | Second network |
|---|---|

| AMPS | MBAA (*X*) | α-keto | DMAAm (*Y*) | MBAA | α-keto |
|---|---|---|---|---|---|
| 1 M | 2, 3, 4 mol% | 1 mol% | 3, 4 M | 0.01 mol% | 0.02 mol% |

158

**Table 2.** Young's modulus ($E_0$), number of monomer units between two crosslinks ($N$), and mesh size ($R_0$) of the first network at its as-prepared state, along with the linear swelling ratio ($\lambda_s$) and mesh size ($R$) of the first network in the as-prepared DN*X*-*Y*.

| DN*X*-*Y* | $E_0$ (kPa) | $N$ | $R_0$ (nm) | $\lambda_s$ | $R$ (nm) |
|---|---|---|---|---|---|
| DN2-4 | 16.2 | 462 | 7.6 | 3.2 | 24.3 |
| DN3-4 | 23.5 | 318 | 6.3 | 2.5 | 15.8 |
| DN4-4 | 33.6 | 224 | 5.3 | 2.2 | 11.7 |
| DN4-3 | 33.6 | 224 | 5.3 | 2.2 | 11.7 |

159

160 **2.2. Sample Geometry.**

161 Dumbbell-shaped samples of various geometries were used to perform uniaxial tensile tests

162 (**Figure 1**). The gauge width *w*, root angle *θ,* gauge length *L*, and thickness *t* were varied, as

163 shown in **Table 3**. Grip width (*Gw*), grip length (*GL*), junction length (*JL*), and total length (*TL*)

164 are changed according to the change in *w*, *θ*, and *L*.GL + JL was fixed at 27.5 mm.

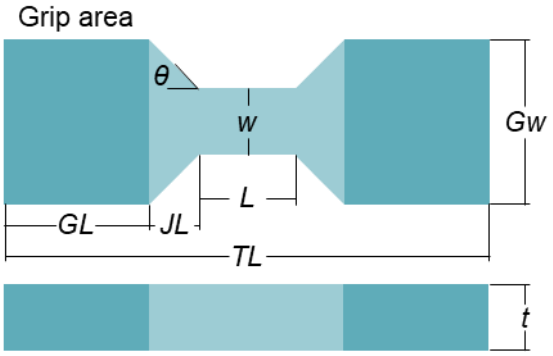


**Figure 1.** The geometry of dumbbell shaped sample. *w*, gauge width; *θ*, root angle; *L*, gauge length; *t*, thickness; *JL*, junction length; *GL*, grip length; *Gw*, grip width; *TL*, total length. GL + JL = 27.5 mm, *TL* = *L* + 55 mm.

Because the damage zone initiation is sensitive to the surface defects of the samples, we adopted a laser cutter (PLS 4.75, manufactured by Universal Laser Systems, Inc., USA) to obtain DN gels with a pre-set geometry. The laser cutter provided a relatively smooth surface, so that the DN gel yielding always began at the root of the dumbbell by stress concentration (for all the investigated samples of more than 100).

**Table 3.** Geometries of DN samples used in this work.

| Dimension | *w* (mm) | *θ* (°) | *L* (mm) | *t* (mm) | *JL* (mm) | *Gw* (mm) |
|---|---|---|---|---|---|---|
| *w*-tuned | 0.75–30 | 45 | 16 | 1.0 | 7.5 | *w* + 15 |
| *θ*-tuned | 10 | 15– | 16 | 1.0 | 7.5 (*θ* ≤ 45), | 10 + 15tan*θ* |

| | | | | | | |
|---|---|---|---|---|---|---|
| ($w$ = 10) | | 75 | | | 7.5/tan$\theta$ ($\theta \geq 45$) | ($\theta \leq 45$), 25 ($\theta \geq 45$) |
| $\theta$-tuned ($w$ = 1.0) | 1.0 | 15–75 | 16 | 1.0 | 7.5 ($\theta \leq 45$), 7.5/tan$\theta$ ($\theta \geq 45$) | 1.0 +15tan$\theta$ ($\theta \leq 45$), 16 ($\theta \geq 45$) |
| $L$-tuned | 10 | 45 | 3.2–32 | 1.0 | 7.5 | 25 |
| $t$-tuned | 10 | 45 | 16 | 1.0–5.0 | 7.5 | 25 |

176

177 **2.3. Tensile Measurements.**

178 Uniaxial tensile tests were performed using an RTC-1310A tensile tester (Orientec, Inc.,
179 Japan) at a sufficiently high tensile velocity (500 mm/min) to reduce the influence of sample
180 dehydration in the air. The tests were performed at least five times for each sample. The nominal
181 stress was calculated as the tensile force divided by the initial cross-sectional area ($w \times t$) of the
182 gauge region, and the nominal strain was calculated as the change in the jig distance divided by
183 the initial gauge length $L$ (**Supporting Fig. 1(a)**). It should be emphasized that because the
184 deformation of the junction area also contributes to the obtained nominal strain, the nominal
185 strain thus obtained contains a large error, especially in the case of a large sample width at a
186 large strain. For typical samples, we calibrated the nominal strain to the actual strain in the
187 gauge region using a video meter (**Supporting Fig. 1(a)**). Specifically, two dots, 8 mm apart,
188 were drawn in the middle of the gauge region as markers, and the distance between the two dots
189 at different stretching ratios was measured using a video camera. The actual strain was
190 estimated from the ratio of the change in distance between the two dots divided by their initial

191 distance. We confirmed that the stress-strain curves before the initiation of the damage zone
192 overlapped for different geometries when using the actual strain obtained (**Supporting Fig.**
193 **1(c)**). For convenience, we use the nominal strain in a later text, unless specifically mentioned.

194

195 **2.4. Birefringence Retardation Measurement.**

196 The birefringence retardation was measured during tensile testing to visually capture the
197 initiation and growth of damage zones in the yielding process. A polarized video camera
198 (CRYSTA PI-1P, Photron Co., Ltd., Japan) was utilized for retardation measurements. The
199 retardation values were represented in color, with color changes following a sequence from
200 blue, light blue, green, yellow, and red as the retardation increased from 0 to 130 nm.
201 Subsequent increases in retardation beyond 130 nm led to color changes in the reverse order.
202 In the case of the DN gels, the observed birefringence retardation primarily stemmed from the
203 orientation of the second network, given that the second network served as the dominant
204 polymeric component [27]. The orientation of the second network was more pronounced in the
205 damage zone where the first network broke compared to the undamaged zone. Consequently,
206 the damage zone could be distinguished from the undamaged regions by the disparity in
207 retardation color. However, in this study, we refrained from providing a quantitative analysis

of the retardation values. This decision was influenced by the strong dependence of retardation on gel thickness, and the accurate measurement of the actual thickness in the damage zone during stretching proved challenging.

## 3. Results and Discussion

### 3.1. Yielding Process and Width Dependence

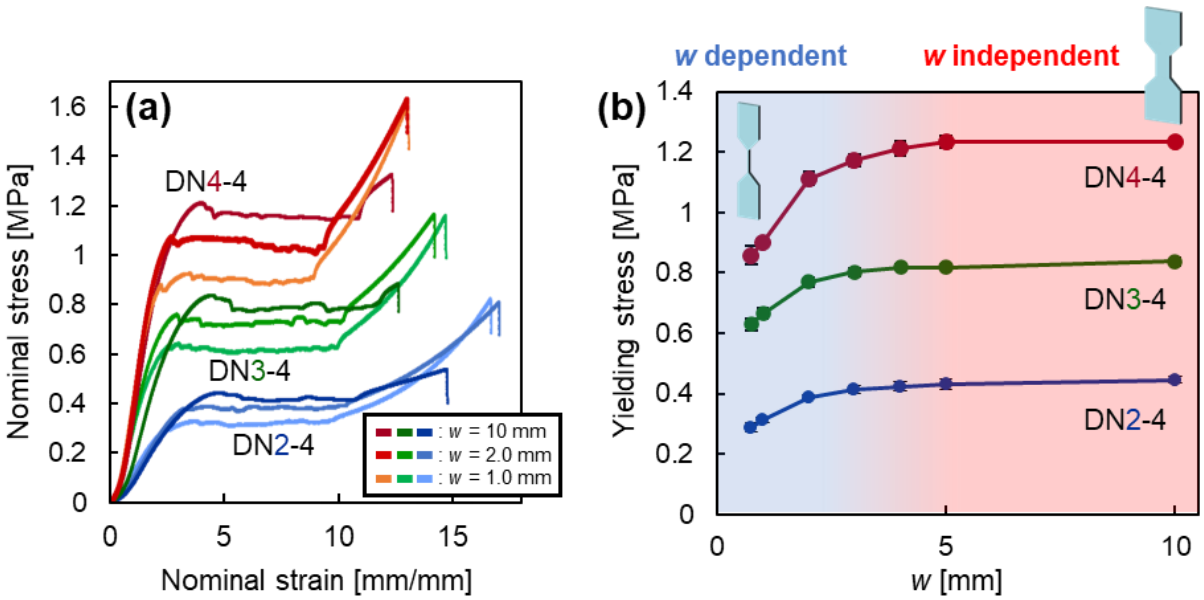


**Figure 2.** Effects of sample width (*w*) on the nominal stress-strain curves **(a)** and yielding stress **(b)** for DN gels of different first network cross-linker density.

Initially, we observed the yielding process in samples with varying widths (*w*). The width

was systematically altered across more than one order of magnitude, ranging from 0.75 mm to 10 mm. The samples maintained a constant root angle (θ) of 45 degrees, a gauge length (L) of 16 mm, and a thickness (t) of 1.0 mm (refer to **Table 2** for details). Tensile stress-strain curves for specific examples, such as DN2-4, DN3-4, and DN4-4 with widths of 1.0, 2.0, and 10 mm, are illustrated in **Fig. 2(a)**. In these examples, the stress increased proportionally with strain, reaching a plateau where the yielding phenomenon became evident. For a given composition, the nominal stress–strain curves exhibited nearly overlapping behavior at small strains, irrespective of *w*, indicating that the deformation before the occurrence of internal fracture in these DN gels is independent of the width. However, in the plateau region, the stress slightly increased with larger sample widths. The yielding point, defined as the point where the nominal stress reaches its maximum value before declining to the plateau stress, is highlighted in **Fig. 2(b)**. The yielding stress is depicted as a function of *w*. It was observed that the yielding stress increased with *w* at small widths and then reached a constant value at larger widths for the three sets of DN gels. This constant yielding stress exhibited an increase with the crosslinker density in the first network. Additionally, the width (*w*) required to reach a constant yielding stress showed an increasing trend as the cross-linker density of the first network increases. These outcomes suggest that *w* plays a crucial role in determining the yielding behavior of DN gels.

It is crucial to note that the relatively distinct deviation in the nominal stress-nominal strain curves before yielding with widths of 10 mm and 1.0 mm (**Fig. 2(a)**) is attributed to differences in the deformation of the samples in the grip regions. Indeed, the two stress-strain curves overlapped when the nominal strain in the gauge region was corrected to the actual strain (see **Supporting Fig. 1**). Due to potential inaccuracies arising from the sample fixation position deviation and deformation in the grip regions, we opt to utilize nominal stress (proportional to the applied force) for subsequent discussions.

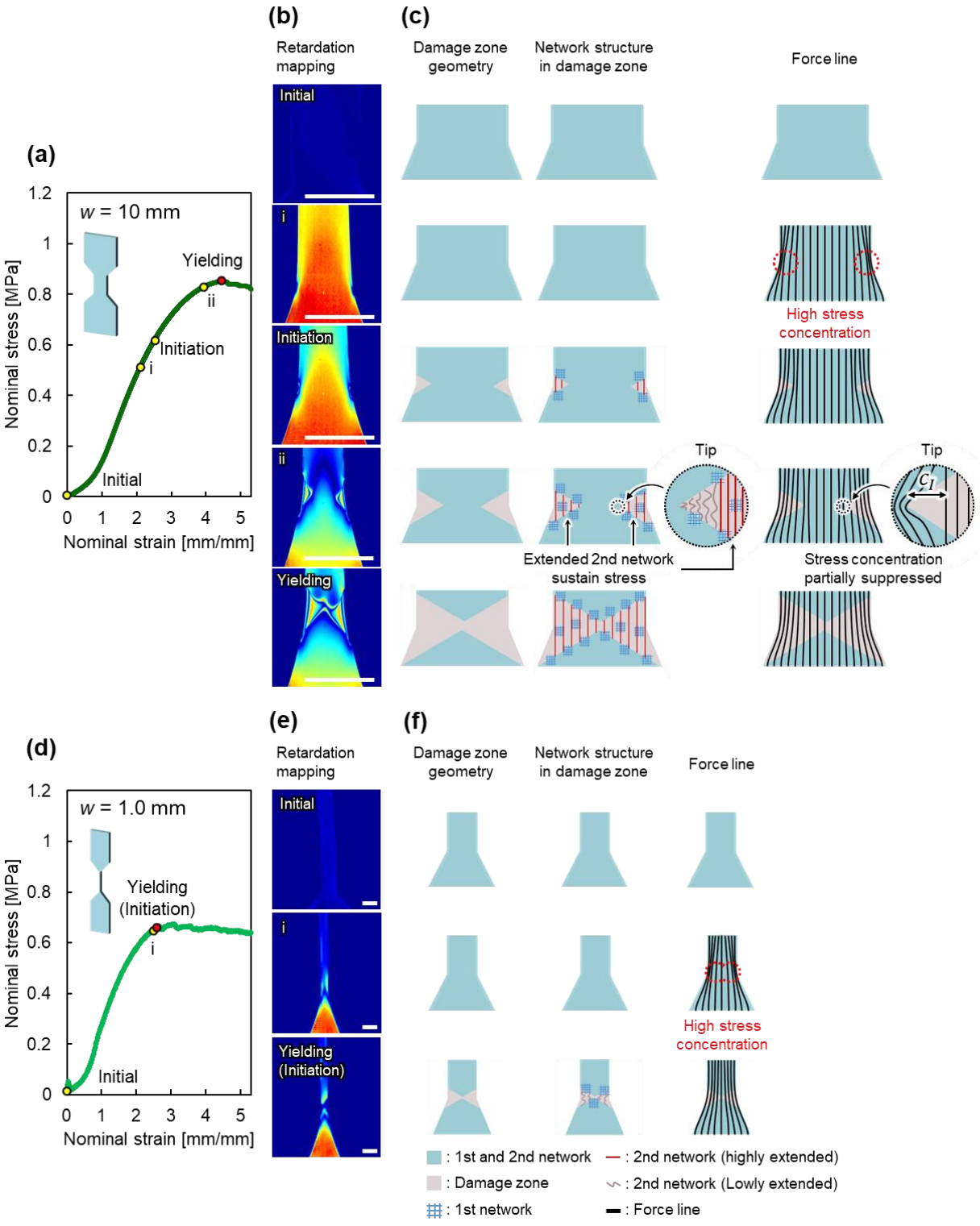
(a)
w = 10 mm
Yielding
ii
Initiation
i
Initial
Nominal stress [MPa]
Nominal strain [mm/mm]
(b)
Retardation mapping
Initial
i
Initiation
ii
Yielding
(c)
Damage zone geometry
Network structure in damage zone
Force line
High stress concentration
Tip
Extended 2nd network sustain stress
Stress concentration partially suppressed
(d)
w = 1.0 mm
Yielding (Initiation)
i
Initial
Nominal stress [MPa]
Nominal strain [mm/mm]
(e)
Retardation mapping
Initial
i
Yielding (Initiation)
(f)
Damage zone geometry
Network structure in damage zone
Force line
High stress concentration
: 1st and 2nd network
: Damage zone
: 1st network
: 2nd network (highly extended)
: 2nd network (Lowly extended)
: Force line

244

245

**Figure 3.** Yielding process of DN gels in the *w*-independent ($w$ = 10 mm) **(a-c)** and *w*-dependent ($w$ = 1.0 mm) **(d-f)** yielding regions. **(a, d)** Stress-strain curves; **(b, e)** Retardation mapping images for each deformation point shown in the stress-strain curves (white scale bars are 10 mm **(b)** and 1.0 mm **(e)**, respectively); **(c, f)** Schematics for damage zone geometry, network structure in damage zone, and force lines for each deformation point shown in **(a, b)** and **(d, e)**. $c_I$ in (**c**) is introduced to characterize the intrinsic effective crack length at the tip of damage zone just before the yielding point of *w*-independent region. Here, "Initial" indicates the point before tensile; "i", indicates the point immediately before the damage zone appears; "Initiation" indicates the onset point that a pair of damage zones is initiated on the two edge surfaces at the root of grip; "ii" indicates the point at which two damage zones grow close to yielding; and "Yielding" indicates the point immediately after two damage zones merge and the yielding stress reaches the maximum. DN3-4 gels were adopted. Other geometry parameters were fixed at $\theta$ = 45°, $L$ = 16 mm, and $t$ = 1.0 mm.

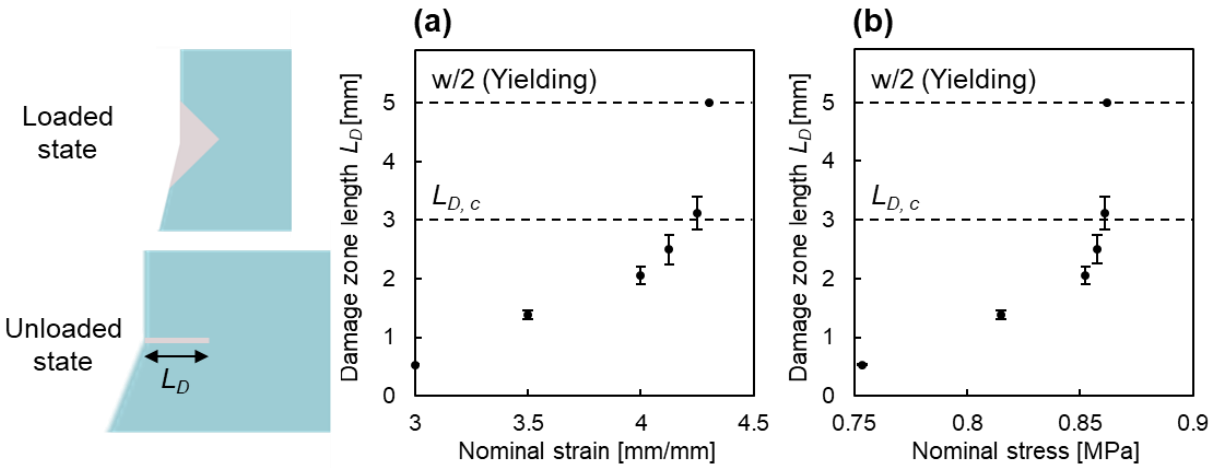


**Figure 4.** Damage zone length $L_D$ evolution with the increase of nominal strain **(a)** and nominal stress **(b)** for *w*-independent sample ($w$ = 10 mm, $\theta$ = 45°, $L$ = 16 mm, and $t$ = 1.0 mm). $L_D$ was measured as damage zone length of width direction for unloaded sample. Above a critical stress/strain, the damage zone length $L_D$ increases rapidly with very small changes in strain and stress, showing a transition from quasi-static fracture to dynamic fracture of the first network. The critical damage zone length ($L_{D,c}$) corresponding to the transition and the yielding point corresponding to $L_D = w/2$ are shown by two dashed lines.

During the tensile tests, real-time birefringence retardation measurements were conducted, revealing the extension of the second network strands due to the internal fracture of the first

network strands [27]. DN3-4 was selected as a representative sample. **Figs. 3(a)** and **(d)** present the stress-strain curves, while **Figs. 3(b)** and **(e)** show representative retardation mapping images corresponding to the positions indicated in the stress-strain curves for samples in the width-independent region ($w$=10 mm) and in the width-dependent region ($w$=1.0 mm), respectively. For the wide sample (**Fig. 3(a, b)**), no internal damage zone was observed macroscopically in the initial stage of stretching (from point "Initial" to "i" in Fig. **3(a)**). When the strain reached a certain value, a pair of damage zones appeared at the two edge surfaces near the root of the dumbbell (at point "Initiation" in **Fig. 3(a)**). Subsequently, as the strain was further increased, the two damage zones grew into a triangle-like shape towards the center of the sample in the width direction (from point "Initiation" to "ii" in **Fig. 3(a)**). During this process, the retardation in the triangular damage zone increased, indicating the extension of the second network. It was observed that when the loading was increased to a critical point, the damage zone growth became very fast, and immediately the two damage zones merged.

To closely examine this auto-accelerated behavior, we investigated the damage zone length $L_D$ along the width direction in response to tensile loading, where $L_D$ was measured for unloaded samples. As depicted in **Fig. 4(a, b)**, $L_D$ gradually increases with loading initially, and then increases rapidly at a certain critical loading, resulting in immediate merge of two damage zones

above a critical stress (or strain). The point labeled “Yielding” in **Fig. 3(a)** aligns with this transition point. This transition phenomenon can elucidate the width dependency of the yield stress observed in **Fig. 2**. The transition point corresponds to a critical damage zone length $L_D = L_{D,c}$, and samples with sufficient width ($w > 2L_{D,c}$) facilitate the rapid growth of the damage zone consistently exhibit the intrinsic yielding stress. Conversely, samples with narrow width ($w < 2L_{D,c}$) display a width dependency of yielding stress.

Therefore, the process of DN gel yielding consists of three steps. The first step involves the initiation of a local damage zone at the edge surfaces near the root of the dumbbell-shaped samples where the stress is concentrated (initiation step). The second step involves the quasi-static growth of the damage zone into the bulk of the hydrogel with further stretching (the growth step). The third step is an auto-accelerated growth of the damage zone above the critical stress/strain (yielding). A further increase in stretching leads to damage zone growth toward the longitudinal direction at constant stress, resulting in necking. In the initiation step, the key factor is the magnitude of stress concentration at the edges. In the growth steps, the key factor is the sample width for damage zone penetration. The latter was clearly observed in a narrow sample. For the narrow sample (**Fig. 3(d, e)**), the initiation of the two damage zones and their merging occurred almost simultaneously, and the points of damage zone initiation and yielding were almost overlapped.

Herein, we discuss the molecular-scale mechanisms. From the force curves and retardation images, we schematically illustrate the damage zone geometry, network structure in the damage zone, and applied force lines in **Figs. 3(c)** and **(f)** for the corresponding points indicated in **Fig. 3 (a, b)** and **Fig. 3 (d, e)** for the wide and narrow samples, respectively. The yielding process is explained as follows: at some point between "i" and "Initiation," the sample's stress concentration near the gauge root makes the first network strands to break, and the crack opening of the first network results in the extension of the second network strands. With substantial extension, the second network strands exhibit strain hardening, which further break the first network in the longitudinal stretching direction along with the extension of the first network crack in the lateral direction, resulting in the formation of a damage zone in the longitudinal direction behind the opened crack **(Fig.3(c)** and **Fig.3(f)**). This process repeats from "Initiation" to "Yielding." Notably, in *w*-independent samples ($w > 2L_{D,c}$) (**Fig.3(c), Fig.4(a, b)**), after the damage zone grows to a certain size ($L_D = L_{D,c}$), the macroscopic stress concentration originating from the gauge root shape becomes adequately negligible due to the additional support from the second network. Subsequently, the destruction of the first network rapidly progresses at the critical stress, corresponding to "Yielding." Therefore, this *w*-independent yielding stress can be recognized as the fracture stress of the first network without the macroscopic stress concentration effect. However, we must additionally consider the effects

of microscopic stress concentration. The triangular shape of the internal damage zone tip and the single damage zone growth path around yielding point (**Fig. 3(b) "ii"**) suggest that some stress concentration remains near the damage zone's tip where the second network could not be extensively stretched (**Fig. 3(c) "ii"**), even though the stress distribution becomes macroscopically homogeneous. In essence, for yielding point of *w*-independent DN gels, the stress concentration is fully eliminated above a certain distance from the damage zone tip but not below this distance. Here, we propose an intrinsic effective crack length $c_I$ for *w*-independent samples to quantitatively characterize such local stress concentration effect. We postulate that the length scale of this critical distance is in the same order of $c_I$ of the damage zone tip at yielding point (**Fig. 3(c), Fig. 4(a, b)**). $c_I$, which influences the intrinsic yielding stress, depends on the microstructure of the DN gels. We will estimate this length $c_I$ later.

On the other hand, when *w* is small and the two damage zones merge before reaching transition point (**Fig. 4(a, b)**), a larger stress concentration in the undamaged central region of the first network results in a smaller yielding stress (**Fig. 2**) as a result of the sample geometry (macroscopic stress concentration).

### 3.2 Root Angle Dependence

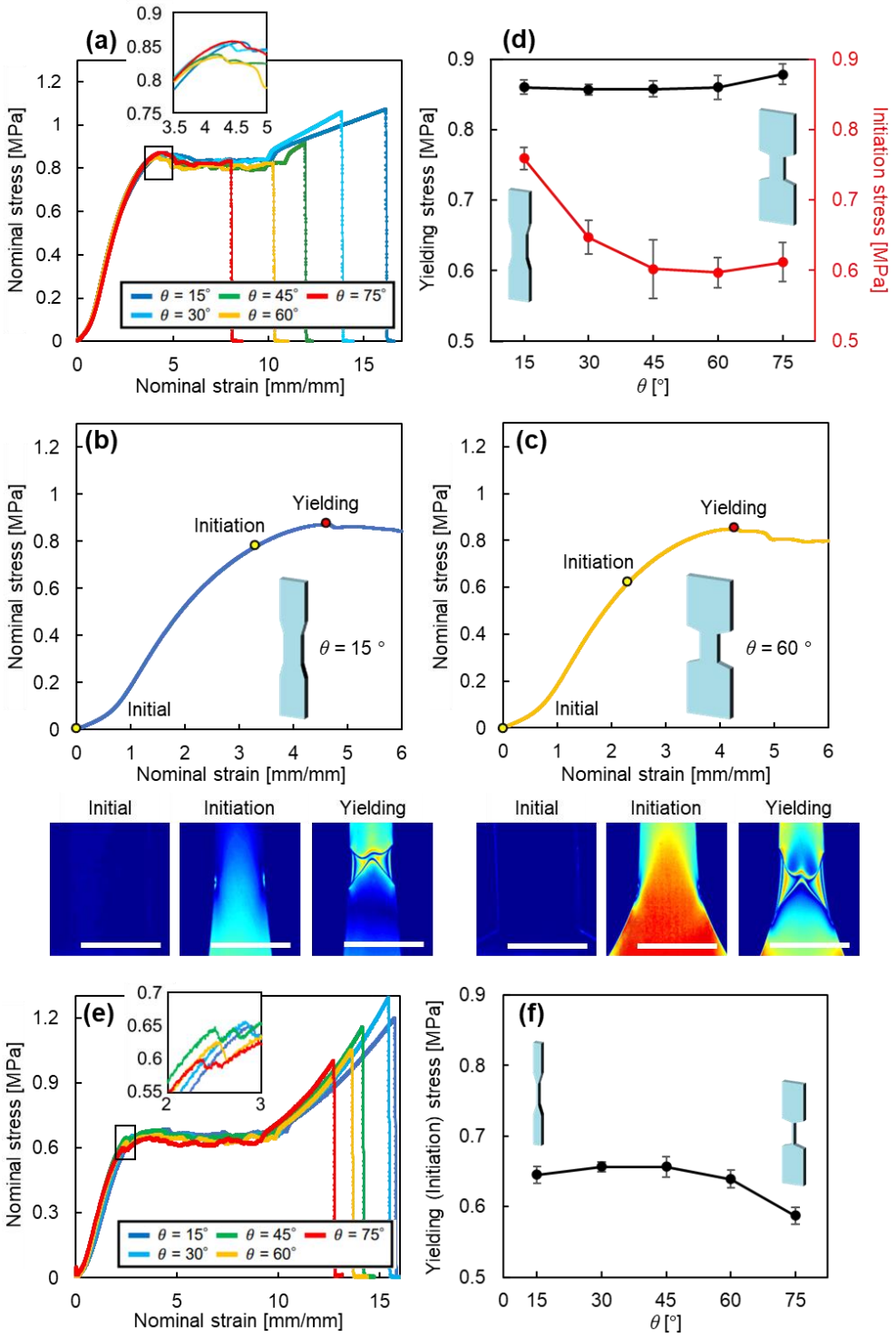


345

346 **Figure 5**. Effects of stress concentration at the gauge roots on the yielding stress and yielding

mechanism. **(a)** Stress-strain curves of DN gels in *w*-independent region ($w$ = 10 mm) with various $\theta$. **(b, c)** Stress-strain curves, and retardation mapping images at each nominal stress of *w*-independent region with $\theta$ = 15° **(b)**, and $\theta$ = 60° **(c)** (Scale bars are 10 mm). **(d)** Yielding stress and stress at yielding initiation (Initiation stress) vs $\theta$ in *w*-independent region. **(e)** Stress-strain curves of *w*-dependent region ($w$ = 1.0 mm) with various $\theta$. **(f)** Yielding (Initiation) stress vs $\theta$ in *w*-dependent region. In these experiments, we used DN3-4 gels with $L$ = 16 mm, $t$ = 1.0 mm.

In the previous sections, we found that damage zone initiation always occurs from the stress concentration area at the roots of dumbbell-shaped samples and that elongation of second network strands results in large damage zone formation, reducing the stress concentration. This stress concentration reduction effect is remarkable for enough wide *w* samples but becomes less effective for narrow *w* samples because the macroscopic stress concentration partially remained at the point where the two damage zones merge. Accordingly, the degree of the macroscopic stress concentration should not influence the intrinsic yielding stress of a wide sample, whereas the yielding stress of a narrow sample should be sensitive to the macroscopic stress concentration. We further verified this conjunction by varying the macroscopic stress concentration. As stress concentration occurs at the root of a dumbbell-shaped specimen [32]

and the root shape of the specimen determines the degree of stress concentration [33], we prepared specimens with five different root angles $\theta$ from 15° to 75° (see **Table 2**) to vary the stress concentration degree. The stress concentration at the edge increases as $\theta$ increases.

The results of the tensile tests in the *w*-independent yielding region ($w$ = 10 mm) are shown in **Fig. 5 (a)**. The stress–strain curves before yielding and the yielding stress (~0.9 MPa) were similar, regardless of the degree of stress concentration. This is consistent with the previous results. Next, we performed birefringence measurements to identify the points of yielding initiation at $\theta$ = 15° (**Fig. 5 (b)**) and $\theta$ = 60° **(Fig. 5 (c)**). Stress at yield initiation (Initiation stress), which is obtained from the retardation mapping images, of the $\theta$ = 60° gel is lower than that of the $\theta$ = 15° gel. The value of the yielding stress and initiation stress as a function of $\theta$ for the *w*-independent yielding region was plotted (**Fig. 5 (d)**). Based on the figure, the initiation stress decreases as $\theta$ increases; however, yielding stress is not affected by $\theta$. In summary, despite the dependence of the initiation stress on the macroscopic stress concentration, the final yielding stress was independent of the stress concentration for the *w*-independent samples. This result indicates that the surface defect, where stress can be highly concentrated, determines the initiation of yielding but does not change the yielding point of the wide samples. Therefore, the effect of defects on the yielding stress of large-width DN gels is negligible. This unique defect-insensitive characteristic allows us to compare the yields of DN gels with different surface

roughness.

We also investigated the effect of $\theta$ on the narrow samples in the *w*-dependent yielding region ($w$ = 1.0 mm) (**Fig. 5 (e)**) and plotted the value of the yielding stress (= initiation stress) as a function of $\theta$ (**Fig. 5 (f)**). The yielding stress decreases with increasing $\theta$. This result is reasonable considering that the initiation and yielding of the narrow samples in the *w*-dependent yielding region nearly overlapped (**Fig. 3(d)**). As the stress concentration at the edge increases with the increase of $\theta$, the stress of damage zone initiation and thereby the yielding stress decrease. Therefore, the yielding stress is defect-sensitive for DN gels with a small *w*.

These results imply that the sample gauge length and thickness do not influence the yield. This was confirmed by tensile tests of DN3-4 with varying *L* and *t*, as shown in **Supporting Figs. 2 and 3**. At least within the sample geometry of this study, these two parameters are negligible. This is because, yielding of DN gels is a local phenomenon and almost free to macroscopic aspect ratio.

### 3.3. Effect of the Second Network Composition

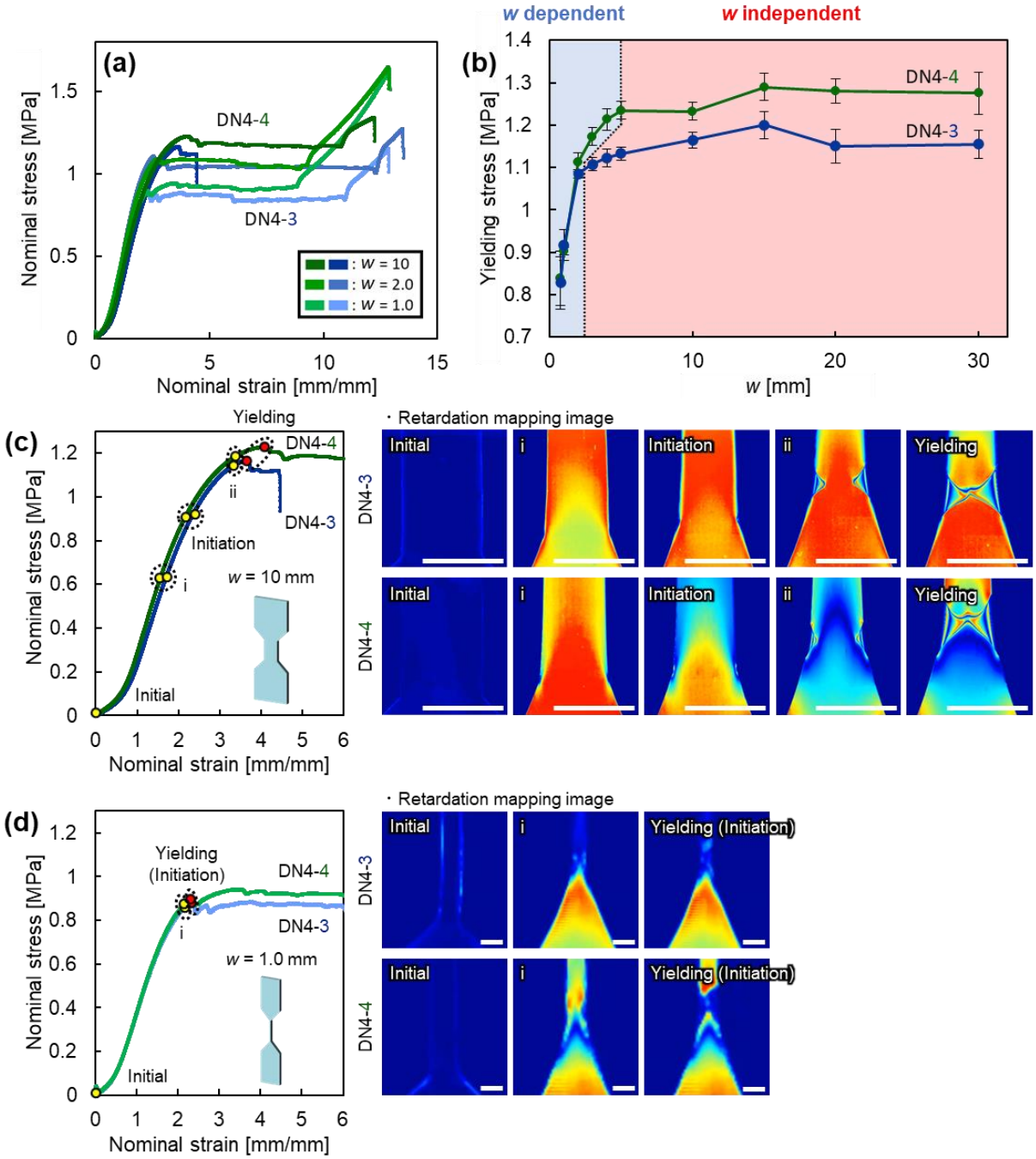


400

401 **Figure 6**. Effects of the second network composition on the *w* dependence of yielding stress

402 and mechanism. **(a)** Stress-strain curves of DN4-3 and DN4-4 with various *w*. **(b)** Yielding

403 stress vs *w*. **(c, d)** Stress-strain curves, and retardation mapping images at each nominal stress

for the DN gels showing *w*-independent yielding (*w* = 10 mm) **(c)** and the *w*-dependent yielding (*w* = 1.0 mm) **(d)** (Scale bars are 10 mm **(c)** and 1.0 mm **(d)**, respectively.).

Next, we focused on the second network composition. We previously concluded that the second network stretching resulted in damage zone formation and later could suppress the macroscopic stress concentration at yielding point for large sample width (*w*-independent region). However, microscopic stress concentration around damage zone tip still remained and we speculated its magnitude related to the two network properties **(Fig. 3 (c))**. Based on this description, it can be inferred that the second network composition affects the yielding behavior. In this section, similar experiments ($w$ = 0.75 ~ 30.0 mm, $\theta$ = 45°, $L$ = 16 mm, $t$ = 1.0 mm) were performed with different second network concentrations. In **Figs. 2 (a)** and **(b)**, when the crosslinker density of the first network is 4 mol%, the largest difference in the yielding stresses of small *w* and large *w* was observed. From the viewpoint of visibility, we use this sample to study the effect of second network concentration. **Fig. 6 (a)** shows the stress-strain curves for gels fabricated with low (DN4-3) and high (DN4-4) second network concentrations with various *w*. Both sets of samples show a similar *w* dependence, intrinsic yielding stress for large *w* samples and a decreasing in yielding stress as *w* decreased before reaching an intrinsic value (**Fig. 6 (b)**). When *w* is less than 2 mm, both DN4-3 and DN4-4 exhibit almost same yielding

422 stress due to macroscopic stress concentration; however, when *w* is greater than 2 mm, DN4-4
423 exhibits a higher yielding stress than DN4-3. Moreover, the minimum width required to show
424 *w*-independent yielding stress slightly increased with the second network concentration.

425 To investigate how the second network influences the intrinsic yielding stress shown in **Fig.**
426 **6(b)**, we conducted birefringence measurements with wide (*w* = 10 mm, **Fig. 6(c)**) and narrow
427 (*w* = 1.0 mm, **Fig. 6(d)**) DN gels. Regardless of the second network concentration difference,
428 the stress-strain curves of DN4-4 and DN4-3 fully overlapped before yielding initiation for both
429 large and small *w*, confirming that the first network mainly carried the load before yielding
430 initiation. During the damage zone growth process of *w*-independent samples, the damage zone
431 tip opening angle of DN4-4 exceeded that of DN4-3, and the damage zone in DN4-4 propagated
432 slower in the lateral direction than that in DN4-3 (see the retardation mapping image in **Fig.**
433 **6(c) ii**). As a result, the critical point for the fast damage zone growth and the fusion of the
434 damage zones, that is, the overall yielding, of DN4-4 occurred later than that of DN4-3. This
435 result indicates that the higher-concentration second network of DN4-4 could carry more load
436 once the first network strands ruptured, and the microscopic stress concentration at the damage
437 zone tip decreased, thereby requiring a relatively larger critical stress and damage zone tip
438 opening angle to propagate the damage zone. Consequently, DN4-4 showed more first network
439 damage at the sample edges in the stretching direction and a higher intrinsic yielding stress than

DN4-3. This explains why DN4-4 exhibited a wider minimum width for *w*-independent yielding than DN4-3. In contrast, small *w* samples in the *w*-dependent region exhibited nearly simultaneous damage zone initiation and merging, as seen from the proximity of initiation and yielding in **Fig. 6(d)**. The second network in the damage zone could not largely suppress the macroscopic stress concentration even at the yielding point. This explains why the yielding stress for the small-width samples did not change with the second network concentration.

It's noteworthy to emphasize that our earlier investigations into the yielding behavior of DN gels utilized samples with $w$ = 2 mm [18,20]. In these studies, the yielding points exhibited minimal variations with changes in the concentration of the second network, resulting in observed yielding stresses slightly below the intrinsic values, and independent of concentration of the second network. Building upon the insights from our current study, we propose that yielding in the prior research probably occurred within the w-dependent region.

In summary, the intrinsic yielding point of DN gels is determined by both the fracture stress of first network and extent of the local stress dispersion facilitated by the second network. The structural characteristics of both networks play a crucial role in this governing mechanism.

### 3.4. Estimation of Intrinsic Effective Crack Length $c_I$

Based on the experimental observations, the quasi-static growth process of the damage zone

458 (step two) in the pre-yielding region homogenizes the stress distribution at the macroscale.
459 When the macroscale stress concentration is fully eliminated, damage zones auto-acceleratingly
460 propagate under constant stress/strain, resulting in intrinsic yielding stress/strain (step three)
461 independent of sample width. However, a microscale stress concentration remains due to the
462 insufficiently stretched second network around the damage zone tip. Consequently, the stress
463 concentration is not completely eliminated, leading to a reduction in the intrinsic yielding stress,
464 as schematically illustrated in **Fig. 3(a-c)**. In **Fig. 7**, we illustrate the evolution of stress
465 distribution with the increase in tensile strain in the pre-yielding region of a DN gel. In the
466 damage zone, the stress is primarily carried by the second network, with the first network
467 fragments acting as slidable crosslinkers. In the undamaged zone, the stress is mainly carried
468 by the first network. Before yielding initiation (points i, ii), stress is fully carried by the first
469 network. At the yield initiation point, the fracture of the first network disrupts the stress balance,
470 causing the damage zone to rapidly advance until a certain distance where the stress balance is
471 restored by the second network load-bearing. Once the damage zone is sufficiently expanded
472 beyond the macroscopic stress concentration zone (point iv), the stress field at the damage zone
473 tip stabilizes into a consistent shape. Therefore, from this point to yield, it is possible to rapidly
474 expand the damage zone with a slight change in stress (**Fig. 4(a, b)**), leading to *w*-independence.
475 This consistent microscopic stress concentration arises from the fact that the second network
476 cannot strain harden near the damage zone tip (**Fig. 3(c)**). The magnitude of stress concentration
477 is an intrinsic material property determined by the composition of the DN gels.

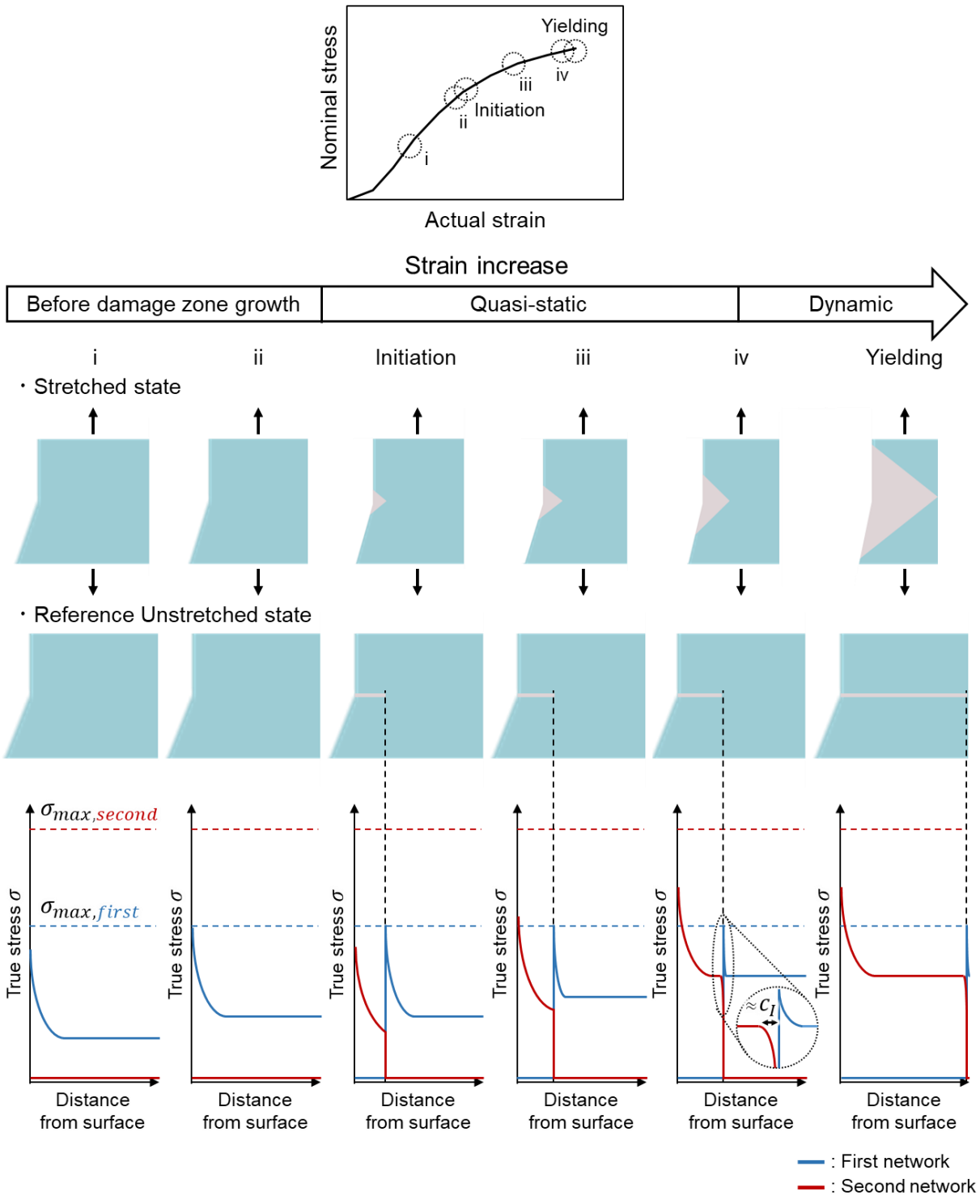
Nominal stress
Actual strain
Yielding
iv
iii
Initiation
ii
i
Strain increase
Before damage zone growth
Quasi-static
Dynamic
i
ii
Initiation
iii
iv
Yielding
・Stretched state
・Reference Unstretched state
$\sigma_{max,second}$
$\sigma_{max,first}$
True stress σ
Distance from surface
$\approx c_I$
: First network
: Second network

478

479

**Figure 7.** Illustration of stress distribution evolution with the increase of tensile strain in the pre-yielding region of a DN gel. Since the stress distribution is symmetric, only the left half of the sample is shown. Upper: sample and damage zone shapes; middle: corresponding sample shapes at reference state; lower: stress distributions along the sample width direction. Each figure corresponds to the indicated strain (i to v) on the stress-strain curve shown at the top of the figure. The solid blue and red curves represent stress carried by the first network and the second network, respectively. The horizontal dashed lines indicate the maximum stress (breaking stress) of the first network (blue) and the second network (red). Although the critical point for the occurrence of fast damage zone growth (point iv) and the yielding point that the damage zones penetrate the whole sample almost overlapped in the stress-strain curve as observed in **Fig. 4(a**, **b**), here we showed these two points separately in the stress-strain curve on purpose for clarity. The intrinsic effective crack length of the first network $c_I$ at the tip of damage zone is defined by **Equation 5** for the yielding point.

We estimate the intrinsic effective crack length $c_I$ at the tip of damage zone from the yielding point to quantitatively characterize this microscopic stress concentration effect. When a material has a crack with a length greater than its crack-insensitive length $\xi$, its strength decreases. According to non-linear elastic fracture mechanics [34,35], the critical energy per unit volume for material failure $W_b$ is proportional to the fracture energy $\Gamma$ of the material and

499 inversely proportional to the crack length $c$ [34,35].

500 $$W_b \simeq \frac{\Gamma}{c} \qquad (c > \xi) \qquad (4)$$

501 In other words, once the crack propagates, $W_b$ decreases with an increase in $c$, which accelerates
502 crack propagation. This equation describes the brittle fracturing of a single network. We applied
503 this theory to the internal fracture of DN gels to estimate $c_I$. When the internal fracture of the
504 first network occurs in the DN gels, the load-bearing of the second network effectively
505 suppresses the stress concentration at the crack tip of the first network, which effectively
506 reduces the internal crack length $c$. In $w$-independent samples near yielding point, the intrinsic
507 effective crack length $c_I$ at the tip of damage zone,

508 $$c_I \simeq \frac{\Gamma_1}{W_{b,y}} \qquad (5)$$

509 Here, $\Gamma_1$ is the fracture energy of the first network, and $W_{b,y}$ is the critical strain energy per unit
510 volume of the first network at yielding. $\Gamma_1$ could be estimated by adopting the Lake-Thomas
511 model [36]. The model proposes that the fracture energy is equal to the number density of
512 polymer strands crossing the crack plane ($v_e$R) multiplied by the energy required to break one
513 bridging strand (= n$N_x U_b$),

514 $$\Gamma_1 \simeq v_e R n N_x U_b \qquad (6)$$

where $v_e$ is the number density of elastically effective strands, $R$ is the end-to-end distance of the strands in the undeformed state, $N_x$ is the monomer number per strand, $n$ is the bond number per monomer in the strand backbone, and $U_b$ is the energy required for breaking one covalent bond on the network backbone. Approximately, $v_e N_x \simeq C_0/{\lambda_s}^3$, where $C_0$ is the monomeric concentration of the first network at its as-prepared state and $\lambda_s$ is the length swelling ratio of the first network in DN gels in relative to its as-prepared state. Therefore, the intrinsic effective crack length $c_I$ relative to the end-to-end distance (mesh size) $R$ of the first network in DN gel is

$$\frac{c_I}{R} \simeq \frac{nU_b C_0}{W_{b,y}{\lambda_s}^3} \qquad (7)$$

A smaller $c_I$/R value indicates more efficient suppression of stress concentration at the first network crack tip by the second network. Here, we estimate $c_I/R$ using experimental parameters $n$ = 2, $\lambda_s$ in **Table 2**, and intrinsic $W_{b,y} \simeq \frac{1}{2}\sigma_y \varepsilon_y$ for $w$-independent region (**Table 4**). Similar to the calculation of $N$ in **Table 1**, we also assumed that $C_0 \simeq 1$ M. Regarding the energy for covalent bond breaking, $U_b$, different values have been used previously [37–39]. Here, we adopt the Gibbs energy barrier $\Delta G^{\ddagger}$ for force-activated bond cleavage [35]. Given a certain timescale of bond breaking (typically 10 s) under a tensile force, $\Delta G^{\ddagger}$ is approximately 80 kJ/mol at room temperature according to the Eyring equation [35]. We estimated $\frac{c_I}{R}$ using $U_b =$ 80 kJ/mol. As shown in **Table 4**, at the yielding point, the intrinsic effective crack length $c_I$ of

533 the first network was suppressed to microscopic values of approximately 10 times the mesh
534 size *R*, independent of the macroscopic internal crack length or damage zone size. We observed
535 that $\frac{c_I}{R}$ increases as the first network cross-linker density increases for a fixed second network,
536 whereas for a fixed first network, $\frac{c_I}{R}$ slightly increases as the second network density decreases.
537 These results further indicate that the increase in the second network's relative strength could
538 more efficiently eliminate the stress concentration at the internal crack tip of the first network
539 and therefore enhance the yielding strength of the DN gels. By utilizing the *R* presented in
540 **Table 2**, $c_I$ is estimated to be in the order of 100 nm for the studied DN gels (**Table 4**).
541 Assuming that $W_b$ reaches the maximum $W_b = W_*$ when the effective crack length reaches
542 mesh size *R* of the network, then $W_*=\Gamma/R$. Thus,

543 $$\frac{W_{b,y}}{W_*} = \frac{R}{c_I} \qquad (8)$$

544 Equation (8) indicates that the yielding strength measured relative to the theoretical maximum
545 strength of the first network is equal to the inverse of $\frac{c_I}{R}$. As shown in **Table 4**, the yield strength
546 was approximately 7–11.5% of the theoretical maximum strength. This result indicates that by
547 increasing the microscopic load-bearing ability of the second network, the yield strength of the
548 DN gel could further approach the maximum value, which provides insight into the design of
549 DN gels.

550

**Table 4.** Intrinsic effective crack length $c_I$ of the first network at the tip of damage zone, estimated from yield point of DN gels of various compositions in relative to its mesh size $R$. Nominal yield stress $\sigma_y$ and actual yielding strain $\varepsilon_y$ were taken from the $w$-independent region ($w$ = 10 mm). $\varepsilon_y$ was measured by video meter.

| DN*X*-*Y* | $\sigma_y$ (MPa) | $\varepsilon_y$ | $\frac{c_I}{R}$ | $c_I$ (nm) | $\frac{W_{b,y}}{W_*}$ |
|---|---|---|---|---|---|
| DN2-4 | 0.44 | 2.55 | 8.7 | $2.1 \times 10^2$ | 0.115 |
| DN3-4 | 0.84 | 2.50 | 9.8 | $1.5 \times 10^2$ | 0.103 |
| DN4-4 | 1.23 | 2.35 | 10.4 | $1.2 \times 10^2$ | 0.096 |
| DN4-3 | 1.17 | 1.90 | 13.5 | $1.6 \times 10^2$ | 0.073 |

551

552

553

554 **4. Conclusion**

555 The pre-yielding process encompasses three distinct steps: (1) initiation of damage zone, (2)
556 quasi-static growth of damage zone, and (3) auto-accelerated expansion of the damage zone.
557 During the quasi-static growth step, the extensively stretched strands of the second network
558 within the damage zone bear a significant load, effectively suppressing stress concentration on
559 the first network near the tip of damage zone. As a result, a larger stress (indicated by a larger
560 damage zone tip opening angle) is necessary for the propagation of the damage zone in the
561 width direction, leading to the rupture of the first network in the stretching direction and the
562 formation of extensive damage zones. In samples with sufficiently large widths, the second

network fully supports the load within the damage zone, completely mitigating macroscopic stress concentration arising from the initial sample geometry of the first network. Further loading prompts auto-accelerated rapid growth of the damage zone under nearly constant stress and strain, culminating in yielding and necking. We define an intrinsic effective crack length ($c_I$) in DN gels for the damaged first network, reflecting the microscopic stress concentration effect that persists in width-independent samples and determining the intrinsic elastic energy per unit volume of the first network at yielding ($W_{b,y}$). The value of $c_I$ is contingent upon the microstructure of the DN gels. For a fixed second network density, an increase in the first network density results in an elevation of $c_I$ relative to the mesh size ($R$) and a reduction in $W_{b,y}$ relative to its theoretical maximum value ($W_*$). Conversely, with a constant first network density, augmenting the second network concentration suppresses local stress concentration, leading to a lower $c_I/R$ or a higher $W_{b,y}/W_*$. Although the DN gel strategy has achieved approximately 10% of the theoretical strength of the first network thus far, there remains room for improvement. The findings of this study contribute to a comprehensive understanding of the yielding process in DN gels and offer valuable insights for the development of even stronger and tougher DN gel materials.

**Acknowledgement**

M.Y., R.K., and J.P.G. perceived the concept, designed the experiments, and interpreted the results. M.Y. performed most of the experiments and analyzed the data. M.Y. and Y.Z. performed birefringence measurements. All authors participated in the discussion. M.Y., R.K., D.R.K. and J.P.G. prepared the manuscript for publication. J. P. G. thanks JSPS KAKENHI (no. 22H04968 and 22K21342). R. K. thanks ambitious special assistant professor program. All the authors thank Chung Yuen Hui for previous comments on the manuscripts.

## References

[1] J.P. Gong, Y. Katsuyama, T. Kurokawa, Y. Osada, Double-network hydrogels with extremely high mechanical strength, Adv. Mater. 15 (2003) 1155–1158. https://doi.org/10.1002/adma.200304907.

[2] Y.H. Na, T. Kurokawa, Y. Katsuyama, H. Tsukeshiba, J.P. Gong, Y. Osada, S. Okabe, T. Karino, M. Shibayama, Structural characteristics of double network gels with extremely high mechanical strength, Macromolecules. 37 (2004) 5370–5374. https://doi.org/10.1021/ma049506i.

[3] Y. Tanaka, R. Kuwabara, Y.H. Na, T. Kurokawa, J.P. Gong, Y. Osada, Determination of fracture energy of high strength double network hydrogels, J. Phys. Chem. B. 109 (2005) 11559–11562. https://doi.org/10.1021/jp0500790.

598 [4] K. Haraguchi, T. Takehisa, Nanocomposite Hydrogels : A Unique Organic-Inorganic
599 Network Structure with Extraordinary Mechanical, Optical, and Swelling/De-swelling
600 Properties, Adv. Mater. 14 (2002) 1120–1124. https://doi.org/10.1002/1521-
601 4095(20020816)14:16<1120::AID-ADMA1120>3.0.CO;2-9.

602 [5] M.K. Shin, G.M. Spinks, S.R. Shin, S.I. Kim, S.J. Kim, Nanocomposite hydrogel with
603 high toughness for bioactuators, Adv. Mater. 21 (2009) 1712–1715.
604 https://doi.org/10.1002/adma.200802205.

605 [6] T. Zhang, T. Zuo, D. Hu, C. Chang, Dual Physically Cross-Linked Nanocomposite
606 Hydrogels Reinforced by Tunicate Cellulose Nanocrystals with High Toughness and
607 Good Self-Recoverability, ACS Appl. Mater. Interfaces. 9 (2017) 24230–24237.
608 https://doi.org/10.1021/acsami.7b06219.

609 [7] T. Sakai, T. Matsunaga, Y. Yamamoto, C. Ito, R. Yoshida, S. Suzuki, N. Sasaki, M.
610 Shibayama, U. Chung, Design and fabrication of a high-strength hydrogel with ideally
611 homogeneous network structure from tetrahedron-like macromonomers,
612 Macromolecules. 41 (2008) 5379–5384. https://doi.org/10.1021/ma800476x.

613 [8] H. Kamata, Y. Akagi, Y. Kayasuga-Kariya, U. Chung, T. Sakai, “Nonswellable”
614 hydrogel without mechanical hysteresis, Science (80-. ). 343 (2014) 873–875.

https://doi.org/10.1126/science.1247811.

[9] A. Sugimura, M. Asai, T. Matsunaga, Y. Akagi, T. Sakai, H. Noguchi, M. Shibayama, Mechanical properties of a polymer network of Tetra-PEG gel, Polym. J. 45 (2013) 300–306. https://doi.org/10.1038/pj.2012.149.

[10] Y. Okumura, K. Ito, The polyrotaxane gel: A topological gel by figure-of-eight cross-links, Adv. Mater. 13 (2001) 485–487. https://doi.org/10.1002/1521-4095(200104)13:7<485::AID-ADMA485>3.0.CO;2-T.

[11] T. Karino, Y. Okumura, C. Zhao, T. Kataoka, K. Ito, M. Shibayama, SANS studies on deformation Mechanism of slide-ring gel, Macromolecules. 38 (2005) 6161–6167. https://doi.org/10.1021/ma050624v.

[12] T. Sakai, H. Murayama, S. Nagano, Y. Takeoka, M. Kidowaki, K. Ito, T. Seki, Photoresponsive slide-ring gel, Adv. Mater. 19 (2007) 2023–2025. https://doi.org/10.1002/adma.200700457.

[13] J.P. Gong, Why are double network hydrogels so tough?, Soft Matter. 6 (2010) 2583–2590. https://doi.org/10.1039/b924290b.

[14] T. Nakajima, T. Kurokawa, S. Ahmed, W.L. Wu, J.P. Gong, Characterization of internal fracture process of double network hydrogels under uniaxial elongation, Soft Matter. 9

(2013) 1955–1966. https://doi.org/10.1039/c2sm27232f.

[15] Y. Tanaka, Y. Kawauchi, T. Kurokawa, H. Furukawa, T. Okajima, J.P. Gong, Localized yielding around crack tips of double-network gels, Macromol. Rapid Commun. 29 (2008) 1514–1520. https://doi.org/10.1002/marc.200800227.

[16] S. Liang, Z.L. Wu, J. Hu, T. Kurokawa, Q.M. Yu, J.P. Gong, Direct Observation on the Surface Fracture of Ultrathin Film, Macromolecules. 44 (2011) 3016–3020. https://doi.org/10.1021/ma2000527.

[17] Y.H. Na, Y. Tanaka, Y. Kawauchi, H. Furukawa, T. Sumiyoshi, J.P. Gong, Y. Osada, Necking Phenomenon of Double-Network Gels, Macromolecules. 39 (2006) 4641–4645. https://doi.org/10.1021/jm00368a001.

[18] T. Matsuda, T. Nakajima, Y. Fukuda, W. Hong, T. Sakai, T. Kurokawa, U. Chung, J.P. Gong, Yielding Criteria of Double Network Hydrogels, Macromolecules. 49 (2016) 1865–1872. https://doi.org/10.1021/acs.macromol.5b02592.

[19] P. Millereau, E. Ducrot, J.M. Clough, M.E. Wiseman, H.R. Brown, R.P. Sijbesma, C. Creton, Mechanics of elastomeric molecular composites, Proc. Natl. Acad. Sci. U. S. A. 115 (2018) 9110–9115. https://doi.org/10.1073/pnas.1807750115.

[20] Y. Zheng, T. Nakajima, W. Cui, C. Hui, J.P. Gong, Swelling Effect on the Yielding,

649 Elasticity, and Fracture of Double- Network Hydrogels with an Inhomogeneous First
650 Network, Macromolecules. (2023). https://doi.org/10.1021/acs.macromol.3c00354.

651 [21] X. Zhao, A theory for large deformation and damage of interpenetrating polymer
652 networks, J. Mech. Phys. Solids. 60 (2012) 319–332.
653 https://doi.org/10.1016/j.jmps.2011.10.005.

654 [22] V. Morovati, M.A. Saadat, R. Dargazany, Necking of double-network gels: Constitutive
655 modeling with microstructural insight, Phys. Rev. E. 102 (2020).
656 https://doi.org/10.1103/PhysRevE.102.062501.

657 [23] I. Riku, K. Mimura, Computational Characterization of Micro-To Macroscopic
658 Deformation Behavior of Double Network Hydrogel, Key Eng. Mater. 525–526 (2012)
659 193–196. https://doi.org/10.4028/www.scientific.net/KEM.525-526.193.

660 [24] Y. Liu, H. Zhang, Y. Zheng, A Micromechanically Based Constitutive Model for the
661 Inelastic and Swelling Behaviors in Double Network Hydrogels, J. Appl. Mech. Trans.
662 ASME. 83 (2016). https://doi.org/10.1115/1.4031897.

663 [25] E. Ducrot, Y. Chen, M. Bulters, R.P. Sijbesma, C. Creton, Toughening elastomers with
664 sacrificial bonds and watching them break, Science (80-. ). 344 (2014) 186–189.
665 https://doi.org/10.1126/science.1248494.

[26] T. Matsuda, R. Kawakami, T. Nakajima, J.P. Gong, Crack tip field of a double-network gel: Visualization of covalent bond scission through mechanoradical polymerization, Macromolecules. 53 (2020) 8787–8795. https://doi.org/10.1021/acs.macromol.0c01485.

[27] K. Fukao, T. Nakajima, T. Nonoyama, T. Kurokawa, T. Kawai, J.P. Gong, Effect of Relative Strength of Two Networks on the Internal Fracture Process of Double Network Hydrogels As Revealed by in Situ Small-Angle X-ray Scattering, Macromolecules. 53 (2020) 1154–1163. https://doi.org/10.1021/acs.macromol.9b02562.

[28] C.T. McKee, J.A. Last, P. Russell, C.J. Murphy, Indentation versus tensile measurements of young's modulus for soft biological tissues, Tissue Eng. - Part B Rev. 17 (2011) 155–164. https://doi.org/10.1089/ten.teb.2010.0520.

[29] M. Rubinstein, R.H. Colby, Polymer Physics, Oxford University Press New York, 2003.

[30] R. Kiyama, M. Yoshida, T. Nonoyama, T. Sedlačík, H. Jinnai, T. Kurokawa, T. Nakajima, J.P. Gong, Nanoscale TEM Imaging of Hydrogel Network Architecture, Adv. Mater. 35 (2023) 1–11. https://doi.org/10.1002/adma.202208902.

[31] S. Cui, C. Liu, Z. Wang, X. Zhang, Single Molecule Force Spectroscopy on Polyelectrolytes : Effect of Spacer on Adhesion Force and Linear Charge Density on Rigidity, (2004) 946–953.

683 [32] L. Feng, I. Jasiuk, Effect of specimen geometry on tensile strength of cortical bone, J.
684 Biomed. Mater. Res. - Part A. 95 A (2010) 580–587.
685 https://doi.org/10.1002/jbm.a.32837.

686 [33] T.L. Anderson, Fracture Mechanics, CRC Press, 2005.

687 [34] R. Long, C.Y. Hui, J.P. Gong, E. Bouchbinder, The Fracture of Highly Deformable Soft
688 Materials: A Tale of Two Length Scales, Annu. Rev. Condens. Matter Phys. 12 (2021)
689 71–94. https://doi.org/10.1146/annurev-conmatphys-042020-023937.

690 [35] R. Long, C.Y. Hui, Crack tip fields in soft elastic solids subjected to large quasi-static
691 deformation - A review, Extrem. Mech. Lett. 4 (2015) 131–155.
692 https://doi.org/10.1016/j.eml.2015.06.002.

693 [36] W.G. City, The strength of highly elastic materials, Proc. R. Soc. London. Ser. A. Math.
694 Phys. Sci. 300 (1967) 108–119. https://doi.org/10.1098/rspa.1967.0160.

695 [37] Y. Akagi, H. Sakurai, J.P. Gong, U. Il Chung, T. Sakai, Fracture energy of polymer gels
696 with controlled network structures, J. Chem. Phys. 139 (2013).
697 https://doi.org/10.1063/1.4823834.

698 [38] S. Wang, S. Panyukov, M. Rubinstein, S.L. Craig, Quantitative Adjustment to the
699 Molecular Energy Parameter in the Lake-Thomas Theory of Polymer Fracture Energy,

Macromolecules. 52 (2019) 2772–2777. https://doi.org/10.1021/acs.macromol.8b02341.

[39] Z.J. Wang, J. Jiang, Q. Mu, S. Maeda, T. Nakajima, J.P. Gong, Azo-Crosslinked Double-Network Hydrogels Enabling Highly Efficient Mechanoradical Generation, J. Am. Chem. Soc. 144 (2022) 3154–3161. https://doi.org/10.1021/jacs.1c12539.

**Pre-Yielding and Necking Process of Double Network Hydrogels Revealed by Sample**

**Geometry Effects**

Masahiro Yoshida[a], Ryuji Kiyama[b,c*], Ye Zhang[a], Daniel R. King[b], Takayuki Kurokawa[b], Jian Ping Gong[b,d*]

[a]Graduate School of Life Science, Hokkaido University, N21W11, Kita-ku, Sapporo 001-0021, Japan;

[b]Faculty of Advanced Life Science, Hokkaido University, N21W11, Kita-ku, Sapporo 001-0021, Japan;

[c]Creative Research Institution (CRIS), Hokkaido University, N21W11, Kita-ku, Sapporo 001-0021, Japan;

[d]Institute for Chemical Reaction Design and Discovery (WPI-ICReDD), Hokkaido University, N21W10, Kita-ku, Sapporo 001-0021, Japan

Corresponding authors: r.kiyama@sci.hokudai.ac.jp; gong@sci.hokudai.ac.jp

# Supporting Information

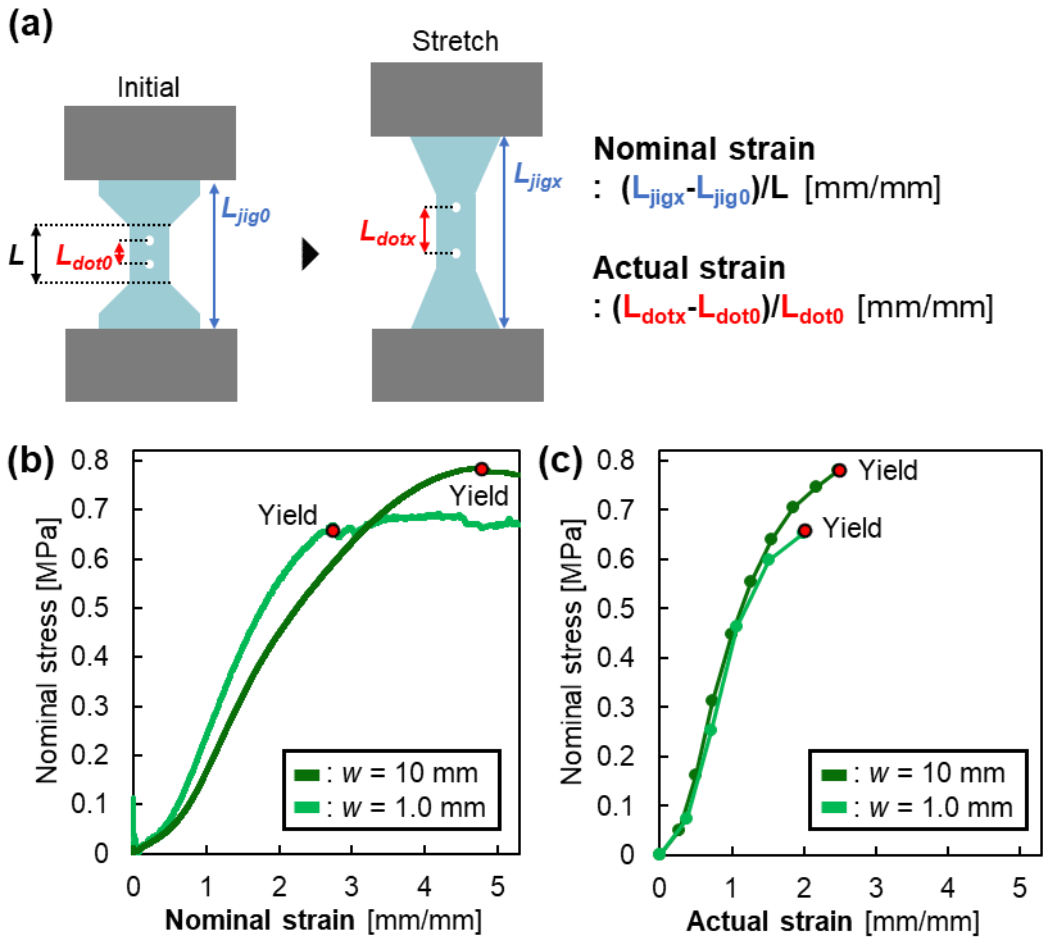


**Supporting Figure 1. (a)** Definition of nominal and actual strain. **(b)** Nominal stress vs. nominal strain and **(c)** nominal stress vs. actual strain curves for DN3-4 gels with widths *w* of 10 mm and 1.0 mm, respectively. For all samples, $\theta$ = 45°, *L* = 16 mm, and *t* = 1.0 mm.

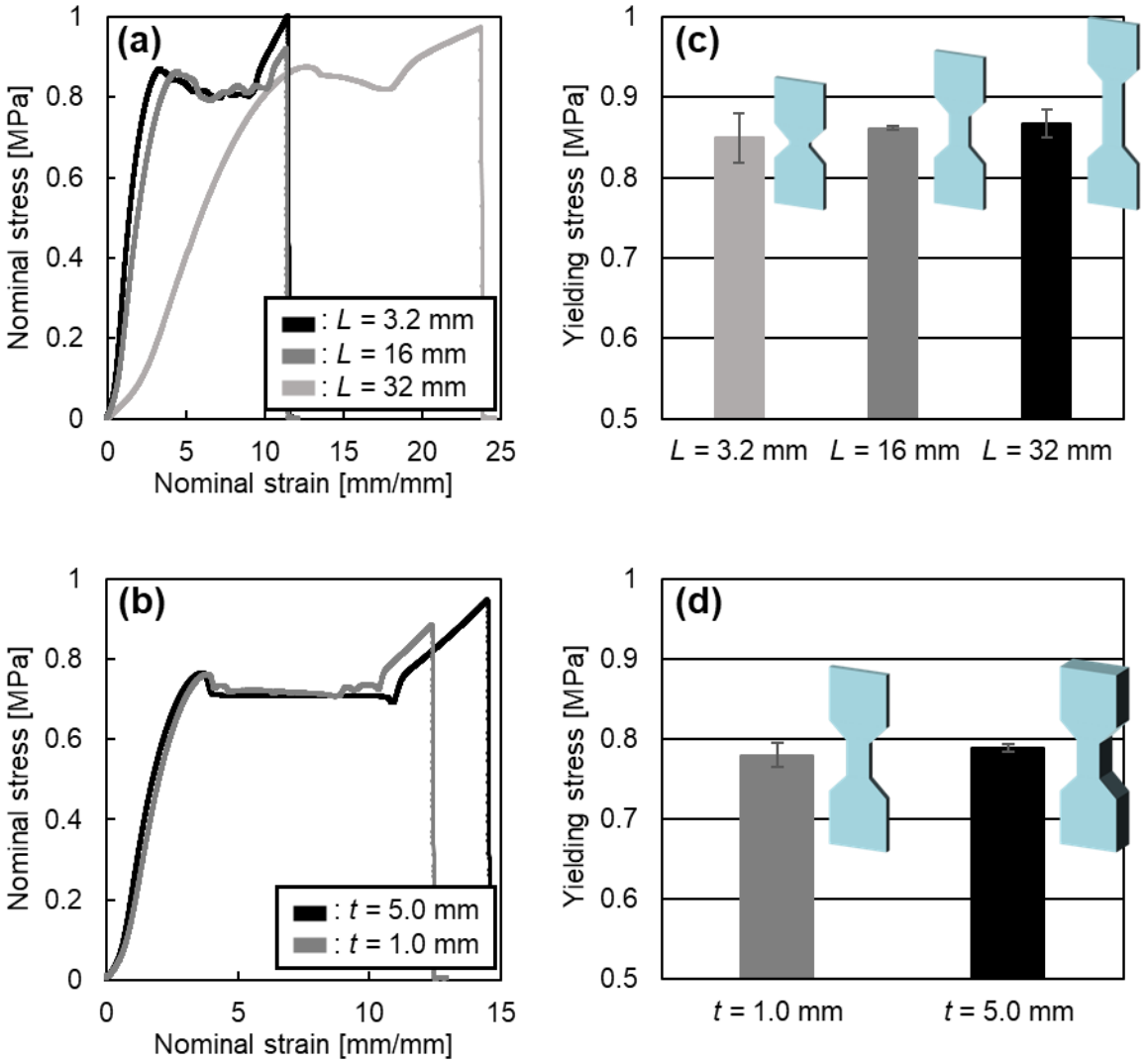


**Supporting Figure 2.** Effects of sample gauge length *L* and thickness *t* on yielding behavior. **(a)** Stress-strain curves of DN-3,4 with various *L* (*w* = 1.0 mm, $\theta$ = 45°, *t* = 1.0 mm). **(b)** Yielding stress vs *L*. **(c)** Stress-strain curves of DN-3,4 gels with various *t* (*w* = 1.0 mm, $\theta$ =

45°, $L$ = 16 mm). **(d)** Yielding stress vs $t$.

Clearly, $L$ and $t$ have no significant effect on the yielding stress of the DN gels. This result is consistent with our observation that the yielding originates from the sample edge and then penetrates the width direction. However, $L$ strongly influenced the strain before yielding. If we made nominal stress-actual strain curves with a length of 3.2 mm, 16 mm, and 32 mm (**Supporting Fig. 3**) to remove the effects of the grip region deformation to the strain, the three curves overlapped. Therefore, we can consider that the strain difference among the three samples with different lengths is derived from the dumbbell grip deformation, and $L$ and $t$ do not significantly change the yielding points.

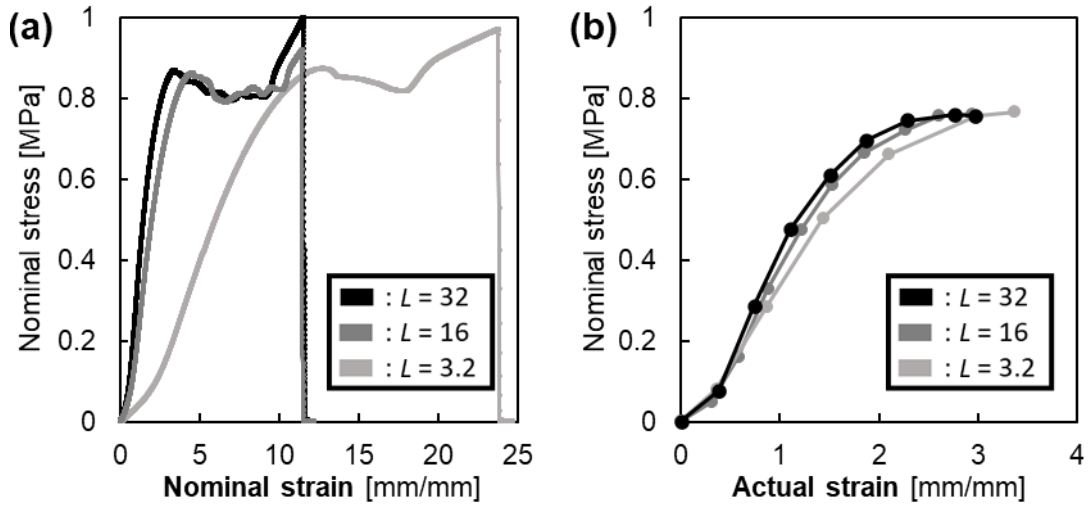


**Supporting Figure 3. (a)** Nominal stress vs nominal strain curves and **(b)** nominal stress vs actual strain curves for a DN3-4 gel with different gauge length L of 32 mm, 16 mm and 3.2 mm ($w$ = 10 mm, $\theta$ = 45°, and $t$ = 1.0 mm).